Steady State Turbulent Transport
in Magnetic Fusion Plasmas

W.W. Lee, S. Ethier, R. Kolesnikov,
W.X. Wang, and W.M. Tang

December 2007

PPPL
PRINCETON PLASMA
PHYSICS LABORATORY
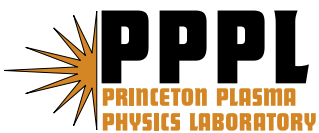
Princeton Plasma Physics Laboratory
Report Disclaimers

PPPL Report Availability

Princeton Plasma Physics Laboratory:

http://www.pppl.gov/techreports.cfm

Office of Scientific and Technical Information (OSTI):

http://www.osti.gov/bridge

Related Links:

U.S. Department of Energy

Office of Scientific and Technical Information

Fusion Links

Steady State Turbulent Transport in Magnetic Fusion Plamsas[*]

W. W. Lee, S. Ethier, R. Kolesnikov, W. X. Wang and W. M. Tang

Plasma Physics Laboratory, Princeton University, Princeton, NJ 08543

For more than a decade, the study of microturbulence, driven by ion temperature gradient (ITG) drift instabilities in tokamak devices, has been an active area of research in magnetic fusion science for both experimentalists and theorists alike. One of the important impetus for this avenue of research was the discovery of the radial streamers associated the ITG modes in the early nineties using a Particle-In-Cell (PIC) code. Since then, ITG simulations based on the codes with increasing realism have become possible with the dramatic increase in computing power. The notable examples were the demonstration of the importance of nonlinearly generated zonal flows in regulating ion thermal transport and the transition from Bohm to GyroBoham scaling with increased device size. In this paper, we will describe another interesting nonlinear physical process associated with the parallel acceleration of the ions, that is found to play an important role for the steady state turbulent transport. Its discovery is again through the use of the modern massively parallel supercomputers.

I.   INTRODUCTION

For the past fifteen years, the studies on Ion Temperature Gradient (ITG) drift instabilities in tokamak devices have been a very active area of research in the magnetic fusion community, contributed by both the theorists and the experimentalists. In this paper, we will only focus on the activities carried out by the researchers using modern supercomputers in simulating ITG modes via Particle-In-Cell codes in a global environment and their discovery of important nonlinear physics responsible for the resulting thermal transport. This understanding is vital for the development in the future of a predictive capability to assess the performance of ITER - an international magnetic fusion project under construction in southern France, for which the US is an important partner. During the period of time mentioned here, after the discovery of the elongated radial structures associated with the ITG modes (streamers) in the early nineties [1], the importance of 1) the $\mathbf{E} \times \mathbf{B}$ nonlinearity for the spatial trapping and de-trapping of the resonant particles [2, 3], 2) the generation of zonal flows [4, 5], and 3) the energy cascade through mode-coupling processes in toroidal geometry [6] have been recognized through high performance computing. However, it is not un-

til recently, with the enormous increase in computational power, that we have the opportunity to examine the role played by the nonlinearity associated with the acceleration of the particles in the velocity space due to the perturbed fields. It is found that this particular nonlinearity, which has mostly been ignored in the fusion community, plays an important role for the generation of zonal flows and the ensuing steady state ion thermal transport. The discovery of this important non-linear physics was made possible only through the use of the most advanced computer platforms available to us such as such as the 6,080-processor IBM SP (Seaborg) at the National Energy Research Scientific Computing Center (NERSC) in Berkeley, CA at the earlier stage of this study [http://www.nersc.gov] and, more recently, the 22,000-core Cray XT3/4 (Jaguar) at the National Center for Computational Sciences (NCCS) in Oak Ridge, TN [http://www.nccs.gov]. In this paper, we will discuss the underpinning physics associated with this nonlinearity and its possible impact on turbulence research for burning plasmas in devices such as ITER.

The microturbulence simulation in the magnetic fusion community has a long history of taking the full advantage of the advances in modern supercomputing. The first simulations of ITG modes were carried out on the then state-of-the-art supercomputer, the Cray C90 at NERSC, using one million particles for simulating a tokamak discharge [1]. As mentioned earlier, the finger-like elongated streamers were observed in the linear stage of the development. However, they were eventually broken up by the turbulence. The measured wavenumber spectra in the turbulent steady state in both the radial (k_r) and poloidal (k_θ) directions agreed with those observed in the tokamak experiments [7] on the Tokamak Fusion Test Reactor (TFTR) at PPPL. Specifically, the k_r-spectrum was peaked at $k_r = 0$ with a width of $k_r \rho_i \approx 0.15$, and k_θ-spectrum was peaked at $k_\theta \rho_i \approx 0.15$ with a width of $k_\theta \rho_i \approx 0.15$ as well. Here, ρ_i is the ion gyroradius. The resulting poloidal spectrum was the result of a downward shift from its peak at $k_\theta \rho_i \approx 0.5$ in the linear stage. These results were one of the first early examples of physics validation between the simulation results and the experimental data for turbulent transport in tokamaks. With the increase in computing power, the importance of nonlinearly generated zonal flows for the evolution of ITG turbulence was further demonstrated by the Gyrokinetic Totoidal Code (GTC) using 100 million particles on the Cray T3E at NERSC [5]. This new physics of zonal flow has been the focus of intense investigation in fusion research ever since, see, for example [8, 9]. Another important discovery using PIC simulation is the transition from Bohm scaling ($\chi_i \propto 1/B$) to GyroBohm scaling ($\chi_i \propto 1/B^2$) using up to 1 billion particles on the IBM SP3 at NERSC [10], where χ_i is the thermal diffusivity for the ions and B is the magnitude of the external magnetic field. This transition

occurs when the minor radius of a tokamak is substantially larger than ρ_i. The GyroBohm scaling is, of course, a good news for the magnetic fusion, since it has a better confinement property. From the simulation point of view, within a ten year span, we have been able to increase the number of particles in the simulation by three orders of magnitude. In doing so, we have greatly improved our understanding of turbulent transport in tokamaks.

The objective of the present paper is to investigate the effects of the velocity space nonlinearity on the physics associated with ITG turbulence described above with particular emphasis on its effects on zonal flows and scaling trends. We will demonstrate that the increase in computational power indeed goes hand in hand with the increase in scientific understanding and discovery.

II. THE GOVERNING EQUATIONS

The governing equations of the simulation are based on the gyrokinetic Vlasov-Poisson equations [11, 13]. In terms of the gyrokinetic units of $\Omega_i(\equiv eB/m_ic)$, $\rho_s(\equiv \sqrt{T_e/T_i}\rho_i)$ for time and space, and $e\phi/T_e$ for the perturbed potential, where ρ_i is the ion gyroradius, they can be written as

$$\frac{\partial F_\alpha}{\partial t} + \frac{d\mathbf{R}}{dt} \cdot \frac{\partial F_\alpha}{\partial \mathbf{R}} + \frac{dv_\parallel}{dt}\frac{\partial F_\alpha}{\partial v_\parallel} = 0, \tag{1}$$

where F is the phase space distribution in the gyrocenter coordinates of $(\mathbf{R} \equiv \mathbf{x} - \boldsymbol{\rho}, \mu_B, v_\parallel)$, α denotes species, $\mathbf{x}$ is the usual spatial coordinate, $\boldsymbol{\rho}$ is the gyroradius,

$$\frac{d\mathbf{R}}{dt} = v_\parallel \hat{\mathbf{b}} + \mathbf{v}_d - \frac{\partial \bar{\phi}}{\partial \mathbf{R}} \times \hat{\mathbf{b}}, \tag{2}$$

$$\frac{dv_\parallel}{dt} = -\hat{\mathbf{b}}^* \cdot \left(\frac{v_\perp^2}{2}\frac{\partial}{\partial \mathbf{R}}lnB + \frac{\partial \bar{\phi}}{\partial \mathbf{R}} \right), \tag{3}$$

$$\mu_B \equiv \frac{v_\perp^2}{2B}(1 - v_\parallel \hat{\mathbf{b}} \cdot \frac{\partial}{\partial \mathbf{R}} \times \hat{\mathbf{b}}) \approx const., \tag{4}$$

$$\hat{\mathbf{b}}^* = \hat{\mathbf{b}} + v_\parallel \hat{\mathbf{b}} \times (\hat{\mathbf{b}} \cdot \frac{\partial}{\partial \mathbf{R}})\hat{\mathbf{b}},$$

$$\mathbf{v}_d = v_\parallel^2 \hat{\mathbf{b}} \times (\hat{\mathbf{b}} \cdot \frac{\partial}{\partial \mathbf{R}})\hat{\mathbf{b}} + \frac{v_\perp^2}{2}\hat{\mathbf{b}} \times \frac{\partial}{\partial \mathbf{R}}lnB,$$

where $\hat{\mathbf{b}}$ is the unit vector in the direction of the external magnetic field, $\parallel$ and $\perp$ are the directions parallel and perpendicular to $\hat{\mathbf{b}}$, respectively. The transformation between the gyrocenter coordinates $\mathbf{R}$ and the usual particle coordinates $\mathbf{x}$ associated with a gyroradius $\boldsymbol{\rho}$ yields

$$\bar{\phi}(\mathbf{R}) = \langle \int \phi(\mathbf{x})\delta(\mathbf{x} - \mathbf{R} - \rho)d\mathbf{x} \rangle_\varphi,$$

where $\langle \cdots \rangle_\varphi$ is the average over the gyro-angle φ. The corresponding gyrokinetic Poisson's equation [11] becomes

$$\tau[\phi(\mathbf{x}) - \tilde{\phi}(\mathbf{x})] = -\bar{n}_i(\mathbf{x}) + n_e(\mathbf{x}), \tag{5}$$

where

$$\tilde{\phi}(\mathbf{x}) \equiv < \int \bar{\phi}(\mathbf{R})F_i(\mathbf{R}, \mu, v_\parallel)\delta(\mathbf{R} - \mathbf{x} + \rho)d\mathbf{R}d\mu dv_\parallel >_\varphi$$

is the second average of the gyro-phase angle φ on the LHS of the equation, which transforms the $\bar{\phi}(\mathbf{R})$ back to the usual coordinates in $\mathbf{x}$. On the RHS, the densities are defined as

$$\bar{n}_\alpha(\mathbf{x}) = \langle \int F_\alpha(\mathbf{R})\delta(\mathbf{R} - \mathbf{x} + \rho)d\mathbf{R}dv_\parallel d\mu \rangle_\varphi, \tag{6}$$

where $\mu \equiv v_\perp^2/2$. Numerically, the transformation between $\mathbf{R}$ and $\mathbf{x}$ can be accomplished through a 4-point average process valid for $k_\perp \rho_i \leq 2$ [15]. The δf method, based on the multiscale expansion between the background and perturbation [14] and utilized for the simulations reported in the present paper, is based on Eqs. (2), (3), (4) and

$$\frac{dw}{dt} = -(1 - w) \left(\kappa \frac{\partial \bar{\phi}}{\partial \mathbf{R}} \times \hat{\mathbf{b}} \cdot \hat{\mathbf{r}} + \frac{T_e}{T_i}(v_\parallel \hat{\mathbf{b}} + \mathbf{v}_d) \cdot \frac{\partial \bar{\phi}}{\partial \mathbf{R}} \right), \tag{7}$$

where $\kappa = \kappa_n - (3/2 - v^2/2v_{ti}^2)\kappa_{Ti}$ is the background inhomogeneity with $\kappa_n \equiv 1/L_n$ and $\kappa_T \equiv 1/L_T$. [Note that the ion acoustic speed c_s is unity in these units.] The perturbed distribution is defined as

$$\delta f_\alpha = \sum_{j=1}^N w_j\delta(\mathbf{R} - \mathbf{R}_{\alpha j})\delta(\mu - \mu_{\alpha j})\delta(v_\parallel - v_{\parallel \alpha j}),$$

where N is the total number of particle ions in the simulation, $F_\alpha = F_{\alpha 0} + \delta f_\alpha$, $F_{\alpha 0}$ is the background Maxwellian with $\int F_{\alpha 0}d\mathbf{x} = 1$,

$$w \equiv \delta f_\alpha/F_\alpha \tag{8}$$

and $F_\alpha \equiv \delta f_\alpha(w_j = 1)$. For the adiabatic electron model, we only follow the evolution of the ion distribution function in time and assume that

$$n_e(\mathbf{x}) = 1 + \begin{cases} \phi(\mathbf{x}), & (m, n) \neq (0, 0), \\ 0, & (m, n) = (0, 0), \end{cases} \tag{9}$$

(m, n) are the poloidal and toroial mode numbers, respectively. The approximation used for n_e is adequate for the studies described in the present paper and $\bar{n}_i$ is given by Eq. (6), where $\bar{n}_{i0} = 1$.

For the modes with $(m, n) \neq (0, 0)$, Eq. (5) can be solved using an iterative scheme [16], whereas, for $(m, n) = (0, 0)$, the gyrokinetic Poisson's equation can be simplified for $k_\perp^2 \rho_i^2 \ll 1$ as

$$\nabla_\perp^2 \phi = -\bar{n}_i + n_e. \tag{10}$$

We should remark here that both Eqs. (5) and (10) are two-dimensional equations perpendicular to the magnetic field.

The parallel nonlinearity, which is taken into account in the present studies, is the last term on the right hand side of Eq. (3). This term has mostly been ignored in the microturbulence community. However, without this term, the energy conservation cannot be satisfied in the simulation [12, 13]. The only other nonlinearity in the simulation, the last term on the right hand side of Eq. (2), called the $\mathbf{E} \times \mathbf{B}$ nonlinearity, which is the nonlinear term most focussed on by the fusion community, since it is responsible for the generation of zonal flows which, in turn, gives rise to the nonlinear saturation of ITG turbulence and it also regulates the steady state transport by breaking up the streamers. We will show in this paper that the nonlinear generation of zonal flows is also greatly influenced by the velocity space nonlinearity.

III.   THE SIMULATION CODE

The gyrokinetic toroidal code (GTC) [5] is a particle-in-cell (PIC) code in global geometry based on the gyrokinetic Vlasov-Poisson equations, Eqs. (1)-(10), where the gyrophase averages associated with $\langle \cdots \rangle_\varphi$ were carried out by representing a gyrokinertic particle as a charged ring [15], and an iterative scheme [16] was used to solve the integral part of the gyrokinetic Poisson's equation, Eq. (5), for $(m, n) \neq (0, 0)$ modes and a direct one-dimensional ODE solver in the radial direction was used for $(m., n) = (0, 0)$ mode for the zonal flows, both in the configuration space. Since the electrons are assumed to be adiabatic, we only push the ions in the code. The code uses the magnetic coordinates (ψ, θ, ζ) to describe a tokamak with a circular cross section, where the concentric flux surfaces are represented by $\psi(r)$ in the radial direction, and θ and ζ are the poloidal and toroidal angles, respectively. On the poloidal plane, a 2D mesh with a uniform but unstrucured grid in ψ and θ is used with Δ (mesh size) $\approx \rho_i$ (ion gyroradius). The code also uses a global field aligned mesh [10, 17], taking advantage of the basic property of microturbulence in tokamaks, i.e., $k_\parallel \ll k_\perp$. As such, the resolution in the toroidal direction is closely related to the resolution in the poloidal direction resulting in a reduction in number for the toroidal grid [10, 18, 19]. A slight

shift of the field lines is then needed in order to match the mesh in the code [10, 20].

Computationally, the code uses one dimensional domain decomposition in the parallel direction for the grid and an additional uniform particle partitioning within each toroidal domain, both implemented with the MPI communication library. Shared memory parallelism is also implemented at the loop level using OpenMP directives, but only for shared memory systems that support multithreading. GTC has been optimized to run efficiently on MPP platforms [20] and the latest results are shown in Fig. 1, where the vertical axis gives the number of particles (in millions) that one can push in one second (wall clock) in one time step and the horizontal axis is the number of processors. This is the so-called weak scaling, where we increase the number of particles in the simulation for a fixed size problem in the 3D configuration space. As one can see, the scaling remains excellent for thousands of processors on various machines, notably Jaguar at ORNL and Blue/Gene/L at IBM Watson. In view of the recent success in the implementation of a second domain decomposition in the radial direction for the GTC grid [21], we believe that this type of scaling will persist for petaflop computing platforms in the future and make gyrokinetic PIC codes a viable tool for plasma simulation for ITER (http://www.iter.org/) - an international collaborative project in France with the US as a major partner. To that end, a new global gyrokinetic PIC code (GTS) in general geometry for shaped plasmas which is capable of handling the interface with actual experiments has recently been developed and optimized for the MPP platforms [19].
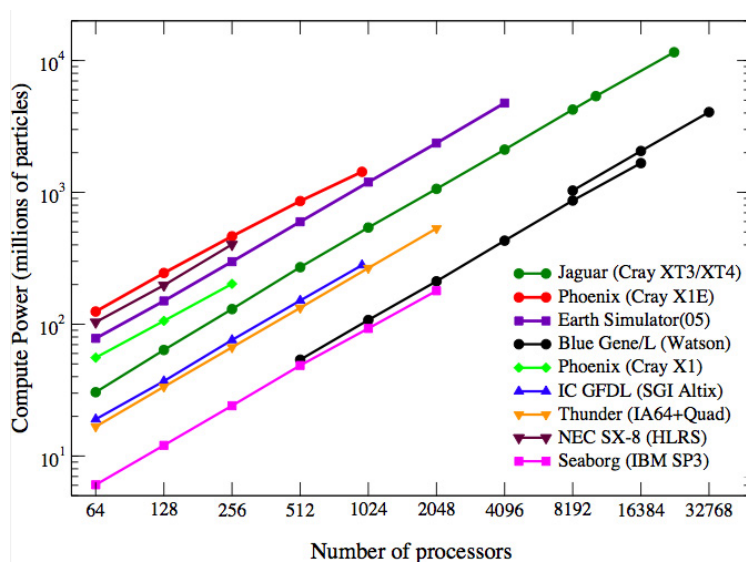
FIG. 1: GTC performance on massively parallel computers.

IV.   THE SIMULATION RESULTS FOR ION TEMPERATURE GRADIENT (ITG) DRIFT TURBULENCE

As mentioned earlier, simulation studies for ITG modes in tokamaks have been a well-researched area since the early nineties. However, the nonlinear evolution and the steady state transport associated with the ITG turbulence are still not well understood. The present paper is intended to shed some light on the related physics using the most up-to-date computing resources available to us. Let us first carry out simulations based on the most complete physics model including all the relevant nonlinearities, i.e., the $\mathbf{E} \times \mathbf{B}$ nonlinearity and the velocity-space nonlinearity. We would like to show that both of these terms are responsible for the observed steady state ion thermal flux for a collisionless plasma. Another related issue is the intrinsic discrete particle noise in PIC codes, which has drawn widespread attention in the fusion community. Specifically, the claim [22], among other things, was that the noise could suppress the steady state flux in ITG turbulence simulations for tokamaks. Although this assertion was contrasted by a later paper based on a self-consistent calculation by extending the fluctuation-dissipation theorem to a nonlinear saturated system [23], the most straightforward way to resolve this issue is to carry out convergence studies in terms of number of particles for the ITG simulations using GTC. Nevertheless, we should mention here that the new study [23] has found that the signal of the relevant modes are order of magnitude higher than the noise in simulation under normal circumstances and no evidence has been found to backup the original assertion [22] that the numerical noise in the shortest wavelength modes can pollute the relevant long wavelength modes in the simulation.

The relevant (Cyclone-based [24]) parameters have been used for the simulation with 64 toroidal grid points for $a/\rho_i = 125$ on each poloidal plane, where a is the minor radius of the tokamak. Thus, the shortest wavelength modes that can be resolved in the code are of the order of $k_\perp \rho_i \approx 1$. The other parameters are: $n_0 = 10, 100, 400, 800$ (number of particles per cell) , $R/L_T = 6.9$, $R/a = 2.79$, $L_n/L_{Ti} = 3.13$, $\Omega_i \Delta t = 7.6$ and $T_e/T_i = 1$, where R is the major radius and Δt is the time step. The radial profile of the inhomogeneity is given by $(1/L)e^{-[(r-r_c)/r_w]^6}$, where L represents either the temperature scale length L_{Ti} or the density scale length L_n with $r_c/a = 0.5$ and $r_w/a = 0.35$. All these runs have been conducted by taking into account of all the physics described in Eqs. (1) - (10), including the nonlinearly generated zonal flows and the velocity space nonlinearity.

The simulation results for $t = 0 - 900a/c_s$ for $15,000$ time steps are shown in Fig. 2 with

solid yellow, blue, red and black lines representing the time evolution for cases using 10, 100, 400 and 800 particles per cell, respectively, where $c_s(\equiv \sqrt{T_e/m_i})$ is the ion acoustic speed and the corresponding gyroradius is $\rho_s(\equiv \sqrt{T_e/T_i}\rho_i)$. These figures describe the time evolution of the ITG turbulence from the linear growth stage to the "sudden" nonlinear saturation ($t \approx 0 - 150a/c_s$), the transition period ($t \approx 150 - 300a/c_s$), and, finally, the turbulent steady state ($t > 300a/c_s$), where various colors correspond to the cases of using various number of particles in the simulation. While the linear growths of these ITG modes are well understood, the phenomenon of "sudden" nonlinear saturation, which has been observed in many previous simulations under different circumstances, e.g., [25–27], remains puzzling. (We will elaborate more on this phenomenon later.) In Fig 2(a), the resulting ion thermal diffusivity is shown, where the steady state value is converged to about $\chi_i \approx 0.5c_s\rho_s^2/a$ in the GyroBohm unit, except for the case of 10 particles per cell (yellow), where the ion thermal diffusivity is enhanced. Most interestingly, the high frequency numerical noise associated with this case is evident in Fig. 2(a). This noise level for the simulation plasma can be estimated by $\sqrt{\langle w_j^2\rangle/N}$ [28], where N is the total number of particles in the simulation and w_j is the weight of the jth particle, Eq. (7). The time rate of change of the volume-averaged square weights for the particles, $\langle\sum_{j=1}^{N} w_j^2\rangle$, as shown in Fig.2 (b), gives us another way to measure χ_i. This quantity is related to the entropy production as first pointed out in Ref. [2], where $w(\equiv \delta f/F)$ in Eq. (8) is related to the volume-averaged thermal flux as

$$\frac{\partial}{\partial t}\sum_{j=1}^{N}(1 - \alpha/4)w_j^2 = \kappa_{Ti}\langle Q_{ir}\rangle,$$

where $\alpha \approx 1$ is related to the velocity space nonlinearity, i.e., the last term on the right hand side of Eq. (3), κ_{Ti} denotes ion temperature inhomogeneity and

$$\langle Q_{ir}\rangle \equiv \frac{1}{N}\sum_{j=1}^{N} w_j v_j^2 \mathbf{v}_{ExB}\cdot\hat{\mathbf{r}}$$

is the ion thermal flux and is related to the ion thermal diffusivity through $\chi_i = \langle Q_{ir}\rangle/(\kappa_{Ti} + \kappa_n)$. Again, Fig 2(b) shows two distinct linear and nonlinear stages of the thermal transport. Moreover, all the runs are converged except for the case with 10 particles per cell (yellow), where the signature of discrete particle noise is apparent, i.e., the steady state flux is higher. In Fig. 2(c) the field energy measured in terms of $e\phi/T_e$ is shown, where the particle noise apparently enhances the fluctuation level (yellow). The time evolution of the zonal flow amplitude expressed in term of v_{ExB}/c_s as given by Fig. 2(d) indicates that the discrete particle noise can give rise to artificial damping of the zonal flows. On the other hand, when a sufficient number of particles
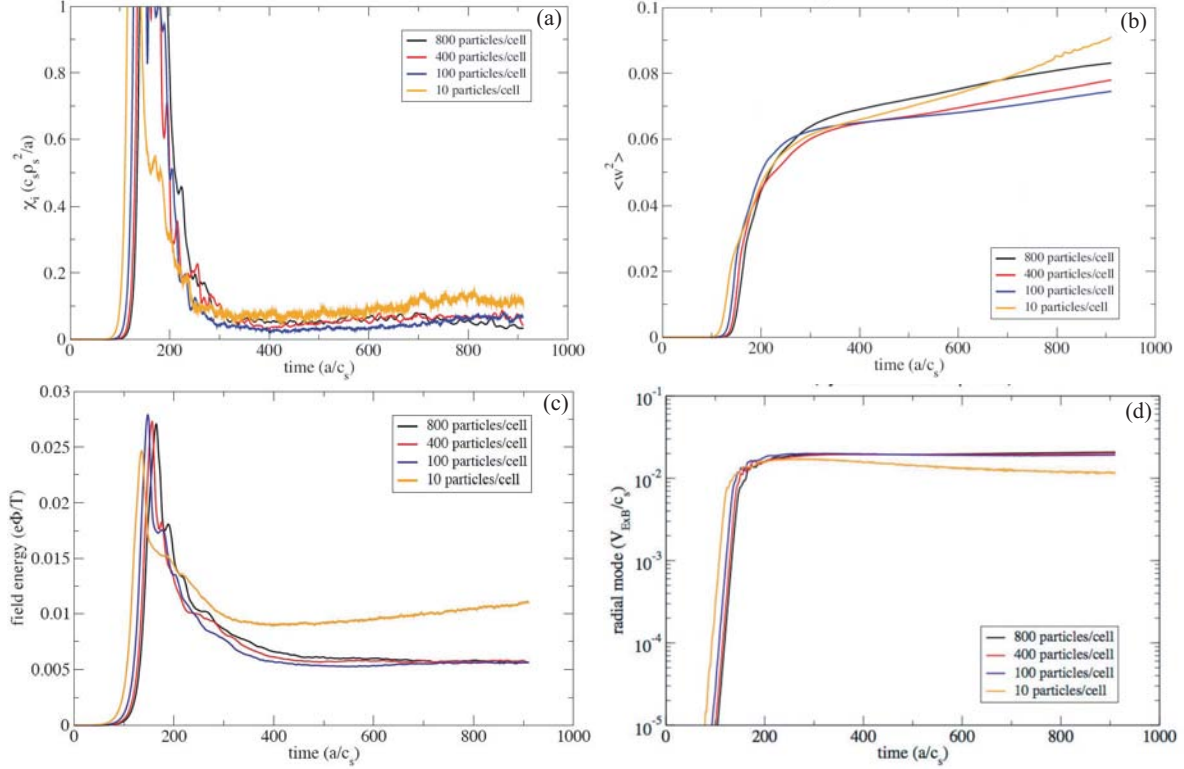
FIG. 2: *Particle number convergence studies for the ITG simulations: time evolution for (a) ion thermal diffusivity, (b) particle weights, (c) field energy, and (d) zonal flow amplitude for cases with 10 (yellow), 100 (blue), 400 (red), and 800 (black) particles per cell.*

is used in the simulation, both the field energy and the zone flow amplitude reach a well defined steady state.

One interesting aspect of these results is the sharp drop of χ_i after the nonlinear saturation as shown in Figs 2(a) and 2(b), which has also been observed in other PIC simulations [25, 27] as well as the continuum simulations with a high velocity space resolution [26]. This property seems to be reasonable since the phase difference between the fluctuating potential ϕ and the perturbed ion density $\delta \bar{n}_i$, which gives rise to the observed χ_i, vanishes suddenly at the saturation and the ion thermal flux drops precipitously in the simulation until the system settles into a new nonlinear relationship between these two quantities in the steady state. However, this unique property did not show up in some of the continuum simulations of ITG modes, which may be related to the use of a coarse velocity space grid [29].

The enhanced fluctuations of $\phi(n = 0, m = 1)$ GAM modes [30] in the simulations reported here have been also observed and the details will be reported elsewhere. In all, we believe that these

high resolution particle simulations of ITG modes, made possible by the availability of the modern day supercomputers, can put to rest the controversy of discrete particle noise in PIC simulations, we hope. The recent assertion that particle noise will come back once the weights of the particles become large is also misleading. Once Landau damping becomes effective in the simulation, usually after a very short transient period in the beginning of the simulation, particle noise can only reside in the normal modes of the simulation plasma and would have negligible effects on physically relevant modes, which are long wavelength modes. The only time particle noise can actually affect the simulation is at the beginning of a conventional (total F) PIC simulation, where the particle random walk caused by the noise can nullify the delicate wave-particle interactions through resonance broadening [15]. As shown in Fig. 2(a), the average particle weight is roughly 0.3 at the end of the simulation. It is conceivable that one can run the simulation until the average particle weight is unity. This happens when an average particle diffuses a distance equivalent to the density or temperature scale lengths, L_n or L_T, of the background inhomogeneity as given by Eq. (7). At this point, the weight will stop growing and the two-scale expansion approximation for the δf method [14] is no longer valid. At any rate, if this becomes a problem in the future, one can always use the recently developed coarse-graining method [31].

In this section, we have presented some of the important convergence issues related to ITG turbulence simulations. Let us now turn our attention to the relative importance of the various nonlinearities responsible for ITG turbulence and it is the topic for the next section.

V. NONLINEAR PHYSICS: DISCOVERY THROUGH COMPUTING

As mentioned earlier, there are two important nonlinear terms governing the nonlinear behavior of the ITG modes, i.e., the $\mathbf{E} \times \mathbf{B}$ term and the parallel acceleration term in Eqs. (2) and (3), respectively. In this paper, through a series of large scale simulations using the most advanced supercomputers, we will show that both of these terms are important in the steady state ITG turbulence, especially when the simulation size is large. This observation, made possible through the availability of high performance computing using a global gyrokinetic PIC code, could have an important impact on our simulation of ITER plasmas in the future.

Let us first re-visit the simulations related to Fig. 2 by using 10 - 20 particles per cell with 32 toroidal planes. By turning on and off the two pieces of nonlinear physics, we have found that the peak χ_i changes dramatically as shown in Fig. 3(a), with the case without either the
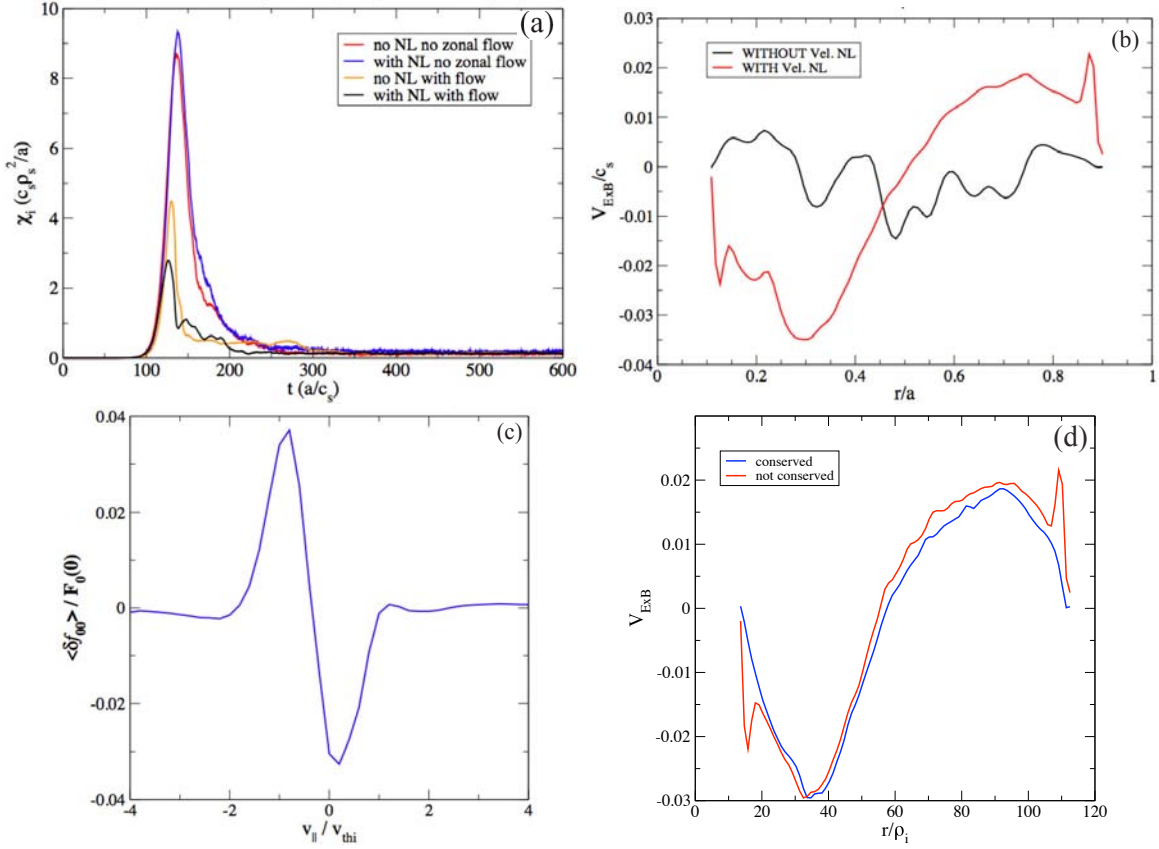
FIG. 3: *(a) Ion thermal flux for $a/\rho = 125$ in the pesence of various nonlinearities, (b) Zonal flow structure, (c) Nonlinear velocity space distribution, and (d) Zonal flow with particle conservation.*

nonlinearly generated zonal flows and the velocity space nonlinearity (red) being much higher at the saturation than the case with both nonlinear physics turned on (black). The run with the presence of the zonal flows, but not with the velocity space nonlinearity (yellow), which is the most prevalent model in the fusion community, is about 50% higher than the case with both terms on (black) at the peak. Moreover, without the presence of zonal flows, the difference is small whether the nonlinear velocity space term is present (blue) or not (red). However, in the nonlinear steady state, all four cases converges to roughly the same level of ion thermal diffusivity as before shown in Fig. 2. This observation for the steady state flux is very similar to that from an earlier study on the effect of this parallel nonlinearity [32]. Furthermore, these new results of ours also validate the earlier global ITG simulations without including the zonal flow physics [1, 25]. In Fig. 3(b), a comparison of the of the radial zonal flow pattern with (red) and without (black) the parallel nonlinearity near the end of the simulation is given. It shows that the zonal flow is global in nature with this extra nonlinearity, and is local without it. This property was first observed by

Villard et al. [33] and it calls into question if one can treat the zonal flows as local short wavelength phenomena. As expected, by activating the parallel nonlinearity, the volume-averaged perturbed distribution, $< \delta f_{00} > [\equiv \sum_{j=1}^{N} w_j \delta(v_{\parallel} - v_{\parallel,j})]$ shows a very broad resonance region that covers a range of $\pm 2 v_{ti}$ at the end of the run as shown in Fig. 3(c), which corresponds to a turbulence-generated parallel flow of $v_{\parallel}/v_{Ti} \approx 2.5\%$. Of course, this flow would vanish without the parallel acceleration. Another interesting question concerning the δf method is that particle conservation is difficult to enforce, which may affect the behavior of the zonal flows. We have carried out a simulation run by setting $\sum_{j=1}^{N} w_j = 0$ and evenly distribute the non-conservation error to all the particles at every time step. The actual difference between with (blue) and without (red) the conservation is rather small as indicated in Fig 3 (d).

Next, let us examine the runs for a larger tokamak with $a/\rho_i = 250$ using 40 particles per cell and 64 toroidal planes, where both the minor radius and the toroidal planes are twice as many as those for the cases in Figs. 2 and 3 . With 1/2 billion particles used in the simulation, these are moderately expensive runs. The results are given in Fiq. 4 (a), where the black line represents the case with both nonlinearities, the yellow line for the case with the zonal flows, but no parallel acceleration, the blue one for the case without the zonal flows, but with the parallel nonlinearity, and the red one for the case without any of the nonlinear effects. With both of the nonlinearities on, the ion thermal diffusivity represented in black reaches the steady state the fastest at the lowest level. The case in yellow is higher in the transition region, but it eventually comes to the same level as the case in black. The case in red corresponds to the results presented in Refs. [1, 25] with a
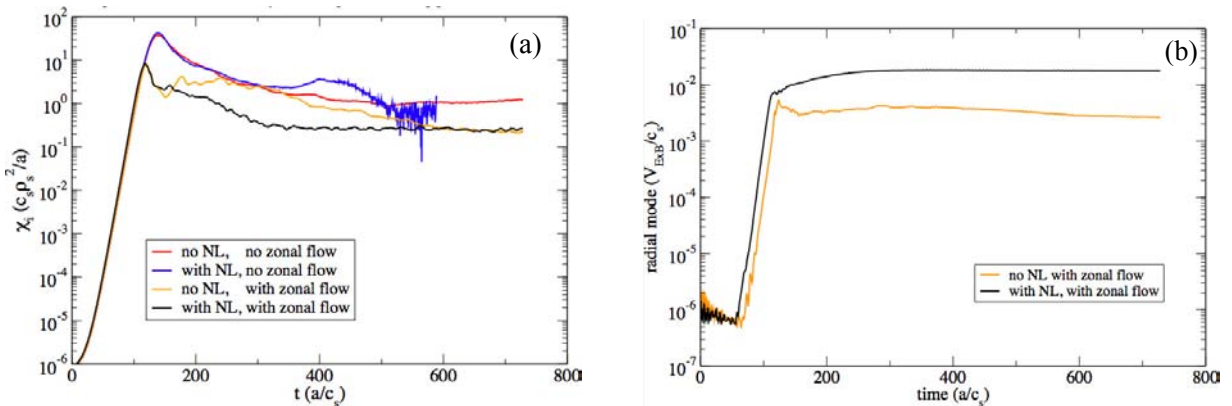
FIG. 4: *(a) The time evolution of the ion thermal flux for $a/\rho = 250$ in the presence of various nonlinearties, and (b) the time evolution of the zonal flows pattern for the cases including only the nonlinearly generated zonal flows with (black) and without (yellow) the velocity space nonlinearity*

much higher level of steady state ion thermal flux, which is expected and was similar to those first pointed out in Ref [5]. The unexpected result is the case with the parallel nonlinearity but without the zonal flows. As shown in blue, it runs into numerical instability. Overall, these results are quite different from those given in Fig. 3, and the only real change in this case is the size of the tokamak in the simulation. The time evolution of the amplitude of the zonal flows for the cases with and without the velocity space nonlinearity is shown in Fig. 4 (b) in black and yellow, respectively. The difference of nearly an order of magnitude in zonal flow amplitude between these two cases in the nonlinear state is quite significant. A better theoretical understanding is urgently needed for a supposedly small nonlinear term, that was ordered out in the Frieman-Chen equation [34], but was kept by others [11–13] for the energy conservation purpose, that can have such an impact on the steady state turbulence. Our interpretation will be given later.

We have also studied the case with $a/\rho_i = 500$ with basically the same parameters as the previous case, i.e., with 40 particles per cell and 64 toroidal planes. But, now we have 2 billion particles in the simulation. Interestingly, all the cases failed due to numerical instabilities during the course of the simulation except for the case when we took both nonlinear effects into account. As shown in Fig. 5 (a), the resulting ion thermal flux reaches a steady state at $t = 400a/c_s$ with $\chi_i = 0.25c_s\rho_s^2/a$. Both Figs. 5(a) and 5(b) indicate that the time evolution are in three distinct stages, i.e., the linear stage, the transition period and the steady state. This is similar to the ones shown in Figs. 2(a) and 2(b). However, one salient feature here is that the transition period is extended in time with a distinct plateau. One possible explanation is that, because of the larger size, the energy cascade to longer wavelength toroidal modes takes a longer time before the simulation reaches a final nonlinear state. Both the perturbed field energy, Fig. 5(c), and the zonal flows, Fig. 5(d), also reached the steady state in the simulation, but, their changes from the transition period are not significant. The resulting zonal flow mode structure at the end of the run is shown in Fig. 5(e). Apparently the global nature of the mode is preserved and there is no evidence that, as ρ_i/a approach zero, the the zonal flow modes would become short wavelength local modes as suggested by the so-called local conjecture, (see, for example, Ref. [32]). The run took about 16.8 hrs on Jaguar at ORNL using 2560 processors (43,000 processor-hours). We believe that these results presented here will have significant impact on our research of plasma microturbulence in the future.

Let us now re-visit the issue of size scaling, as was first investigated by a truly global simulation code [10]. The basic difference for the present study is the presence of the velocity space
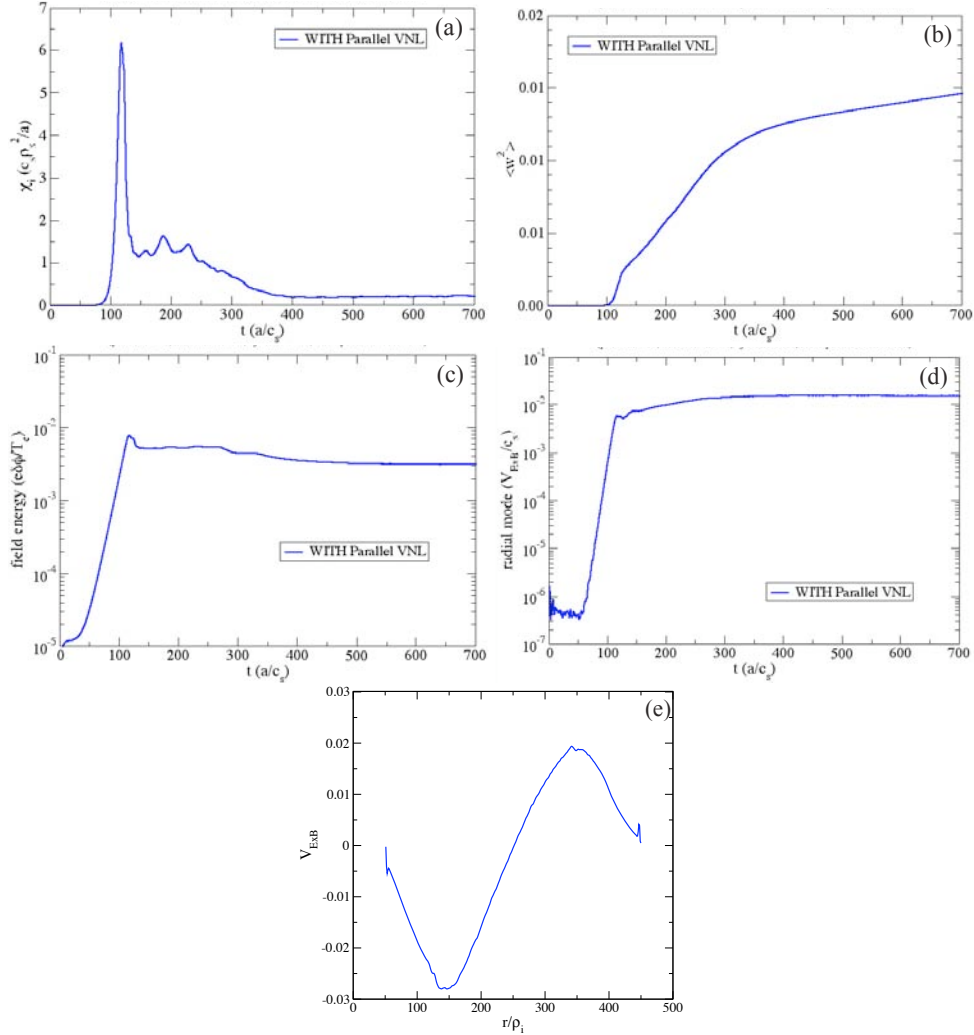
FIG. 5: *Time evolution of (a) the ion thermal flux, (b) the particle weights, (c) the field energy, and (d) the radial modes, as well as (e) the zonal flow structure for $a/\rho = 500$ including both the nonlinearly generated zonal flows and the velocity space nonlinearity.*

nonlinearity, which was not considered earlier. Without it, the zonal flows were dominated by short wavelength modes [5], rather than the global mode structure as shown in Fig. 3(b). The ion thermal diffusivities for the three cases of $a/\rho_i = 125, 250$, and 500 are plotted in Fig. 6. As one can see, these results seem to indicate that the transition from Bohm to GyroBohm scaling takes place around $a/\rho_i \approx 500$ similar to the previous study [10], although the actual thermal diffusivities from the present study are an order of magnitude lower. The sizes corresponding to the actual tokamak experiments of DIIID at General Atomics, Inc. (GA), NSTX at Princeton Plasma Physics Laboratory (PPPL), TFTR also at PPPL (now dismantled), and ITER are also shown in Fig. 6.
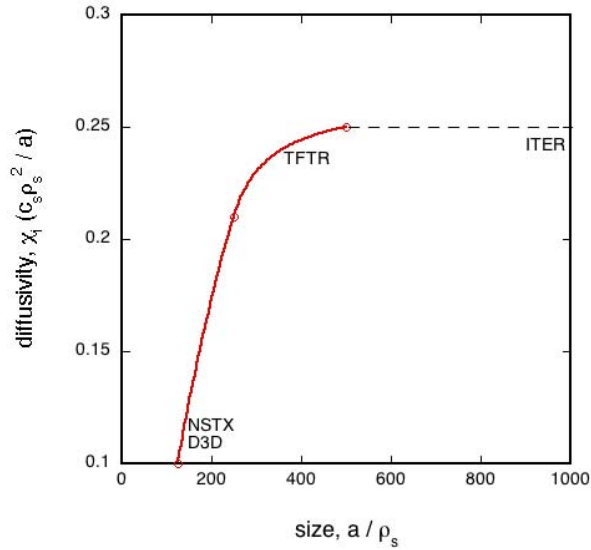
FIG. 6: Transition from Bohm to GyroBohm

Thus, ITER is well into the GyroBohm regime, which is a good news.

The difference in the magnitude of χ_i presented here in comparison with those given earlier in Ref. [10] needs more discussion. The fact that the earlier study ignored the velocity space nonlinearity was not the only difference. That study has also included a heat bath of the form of $\delta f_c = -F_{i0}[(v/v_{Ti})^2 - 3/2]\delta T/T_i$ in the code to prevent profile relaxation. This term is not included in our simulation. This difference may also be related to the numerical difficulty that we encountered for the case of $a/\rho_i = 500$ when only the zonal flows were kept in the code without the velocity space nonlinearity. This nonlinearity might be needed to provid the additional collisionless dissipation in the simulation. The fact that the velocity space nonlinearity has played such an important role here may be understood from the point of view of gyrokinetic ordering [11, 12]. Specifically, from Eqs. (2) and (3), one can see that the wavelengths for both the zonal flows and the parallel perturbations are related to the device size, i.e., a (minor radius) and R (major radius), respectively. As such, these terms, i.e., $k_\perp \phi$ and $k_\parallel \phi$ are of the same order from the point of view of gyrokinetic approximation. Therefore, they are on the same footing and should be kept in the simulation. But, of course, more theoretical understanding on this issue is also needed.

VI. CONCLUSIONS

We have conducted extensive numerical studies on the nonlinear physics related to microturbulence in tokamaks on the modern-day supercomputers. This study is only possible with the availability of the computing resources at the National Energy Research Supercomputing Center at Lawrence Berkeley National laboratory and at the National Center for Computational Sciences (NCCS) at Oak Ridge National Laboratory. The important nonlinear physics related to the zonal flow generation in the configuration space and the parallel acceleration in the velocity space has been identified through large scale computing made possible by using these computing resources.

There are many other global gyrokinetic PIC codes for studying core turbulence in tokamaks such as GT3D [35], GEM [36], GTC-S [19], and ORB5 [37] as well as the global continuum codes such as GYRO [38] and GYSELA [39]. Hopefully, the results presented here using GTC [5] will start a genuine verification exercise worldwide to sort out the differences, the similarities, and, most importantly, the applicability of these codes. One of the important issues for the steady state transport is the effect of profile relaxation due to energy diffusion, which will be addressed in a separate publication [40]. On the other hand, the physics associated with the stationary spectra at low (m, n) modes for the steady state ITG turbulence remains unresolved and needs attention.

VII. ACKNOWLEDGMENT

[1] S. E. Parker, W. W. Lee, and R. A. Santoro, Phys. Rev. Lett. **71**, 2042(1993).

[2] W. W. Lee and W. M. Tang, Phys. Fluids **31**, 612 (1988).

[3] S. E. Parker et al., Phys. Plasmas **1**, (5): 1461 (1994).

[4] M. A. Beer et al., Phys. Plasmas **4**, 1792 (1997).

[5] Z. Lin, T. S. Hahm, W. W. Lee, W. M. Tang and R. White, *Science*, **281**, 1835 (1998).

[6] W. X. Wang et al., Phys. Plasmas **14**, 072306 (2007).

[7] R. Fonck et al., Phys. Rev. Lett. **70**, 3736 (1993).

[8] P. H. Diamond et al., Plasma Phys. Contr. Fusion **47**, R35 (2004).

[9] K. Itoh et al., Phys. Plasmas **13**, 055502 (2006).

[10] Z. Lin, S. Ethier, T. S. Hahm, W M. Tang, Phys. Rev. Lett. **88**, 195004 (2002).

[11] W. W. Lee, Phys. Fluids **26**, 556 (1983).

[12] D. E. Dubin, J. A. Krommes, C. Oberman and W. W. Lee, Phys. Fluids **26**, 3524 (1983).

[13] T. S. Hahm, Phys. Fluid **31**, 2670 (1988).

[14] S. E. Parker, and W. W. Lee, Phys. Fluids B **5**, 77 (1993).

[15] W. W. Lee, J. Comp. Phys. **72**, 243 (1987).

[16] Z. Lin and W. W. Lee, Phys. Rev. E **52**, 5646 (1995).

[17] A. M. Dimits, Phys. Rev. E **48**, 4070 (1993).

[18] B.Scott, Phys. Plasmas. **5**, 2334 (1998).

[19] W. X. Wang et al., Phys. Plasmas **13**, 092505 (2006).

[20] S. Ethier, W. M. Tang, and Z. Lin, J. Phys.: Conf. Series **16**, 1 (2005).

[21] M. F. Adams, S. Ethier, and N. Wichmann, Journal of Physics: Conference Series, **78**, 012001 (2007).

[22] W. M. Nevins, G. W. Hammett, A. M. Dimits, W. Doralnd, and D. E. Shumaker, Phys. Plasmas **12**, 122305 (2005).

[23] T. G. Jenkins and W. W. Lee, Phys. Plasmas **14**, 032307 (2007).

[24] A. M. Dimits, G. Batemen, M. A. Beer et al., Phys. Plasmas **7**, 969 (2000).

[25] W. W. Lee and R. A. Santoro, Phys. Plasmas **4**, 169 (1997).

[26] T. H. Watanabe and H. Sugama, Nucl. Fusion **46**, 24 (2006).

[27] J. L. V. Lewandowski, G. Rewoldt, S. Ethier, W. W. Lee, and Z. Lin, Phys. Plasmas **13**, 072306 (2006).

[28] W. W. Lee, J. Lewandowski, T. S. Hahm, and Z. Lin, Phys. Plasmas **8**, 4435 (2001).

[29] J. Candy and R. E. Waltz, Phys. Plasmas **13**, 032310 (2006).

[30] M. N. Rosenbluth and F. L. Hinton, Phys. Rev. Lett. **80**, 724 (1998).

[31] Y. Chen and S. E. Parker, Phys. Plasmas **14**, 082301 (2007).

[32] J. Candy, R. E. Waltz, S. E. Parker and Y. Chen, Phys. Plasmas **13**, 074501 (2006).

[33] L. Villard et al., Plasma Phys. Contol. Fusion **46**, B51 (2004).

[34] E. A. Frieman and L. Chen, Phys. Fluids **25**, 502 (1982).

[35] Y. Idomura, S. Tokuda and Y. Kishimoto, Nucl. Fusion **43**, 234 (2003)

[36] Y. Chen and S. E. Parker, J. Comp. Phys. **189**, 463 (2003).

[37] S. Jolliet et al., Comp. Phys. Comm. bf 177, 409 (2007).

[38] J. Candy and R. E. Waltz, J. Comp. Phys. **186**, 545 (2003).

[39] V. Grandgirard et al., J. Comp. Phys. **217**, 395 (2006).

[40] R. Ganesh, W. W. Lee, S. Ethier and J. Manickam, manuscript in preparation.